Measuring the complete set of spatial Schmidt modes of entangled two-photon fields

Radhika Prasad,[1,*] Nilakshi Senapati,[1] Abhinandan Bhattacharjee,[2] Suman Karan,[1] and Anand K. Jha[1,†]

[1]*Department of Physics, Indian Institute of Technology Kanpur, Kanpur, Uttar Pradesh 208016, India*

[2]*Paderborn University, Warburger Straße 100, 33098, Paderborn, Germany*

(Received 27 October 2025; revised 21 August 2026; accepted 23 September 2026; published 30 October 2026)

Spontaneous parametric down-conversion (SPDC) is the most widely used source of high-dimensional entangled two-photon states, and the entanglement in the spatial degree of freedom is considered best suited for harnessing high-dimensional advantages. Although the Schmidt basis provides a natural choice for state characterization of entangled two-photon states in any degree of freedom, the existing techniques can only reconstruct the Schmidt spectrum when the Schmidt basis is known *a priori*. There is currently no technique that can measure the unknown Schmidt basis of an entangled two-photon state. In this paper, we present a technique that measures the complete set of spatial Schmidt modes without any prior knowledge of the Schmidt basis, as long as the cross-spectral density functions corresponding to individual photons are of Schell-model type. Using this technique, we report measurement of states with over 3000 Schmidt modes—highest reported yet—with up to 98% fidelity. Our technique works even when the entangled field is very low-dimensional or entirely separable, as well as when the field pumping the SPDC is structured. We expect our work to significantly advance harnessing of spatial entanglement.

DOI: 10.1103/rwmz-jp7r

I. INTRODUCTION

High-dimensional entangled states offer increased information capacity [1,2] and noise resilience [3,4] that are crucial for quantum information protocols including quantum cryptography [5–7]. Spontaneous parametric down-conversion (SPDC) is the most widely used method for generating high-dimensional pure entangled two-photon states [8–11]. Although SPDC photons are rendered entangled in several degrees of freedom, the entanglement in the spatial degrees of freedom [12–15] is considered best suited for harnessing high-dimensional advantages [16,17]. It is known that for pure two-photon states, the natural basis for measuring and characterizing entanglement as well as maximizing mutual information [18] is the Schmidt basis [19–22]. The representation of an entangled state in terms of Schmidt modes is referred to as the Schmidt decomposition [19,23], and the weightage of the modes is called the Schmidt spectrum. However, due to the lack of efficient techniques for measuring high-dimensional spatial Schmidt basis, the entanglement in the spatial degree of freedom has been mostly explored in bases that are either measurement-convenient, such as the pixel basis [24,25] or the bases for which the detectors are readily available [26–30].

In the last two decades, there have been several theoretical works on the Schmidt decomposition of SPDC photons. Analysis of high-dimensional spatial entanglement in the Schmidt basis was first presented by Law and Eberly within certain stringent SPDC phase-matching approximations [20]. The subsequent works made less stringent approximations [18,31,32] and worked out Schmidt decomposition even at propagation distances away from the plane of the crystal producing SPDC [8]. The experimental progress toward measuring the Schmidt decomposition has been very limited. In the high-gain SPDC, which involves multiple photons in the signal and idler modes, there is a technique for measuring the Schmidt modes using intensity-intensity [33] or joint correlation measurements [34]. However, in the low-gain SPDC, the available techniques can measure the Schmidt spectrum of entangled two-photon fields only when the Schmidt basis is known. For example, experimental techniques have been developed for measuring the Schmidt spectrum in the OAM basis [14,15,29], and also in the one-dimensional and two-dimensional transverse momentum bases [23,35–37]. Some of these measurement techniques employ single-mode fibers [14,23,37] for light collection and suffer from poor mode-dependent coupling efficiency [30,38]. Many other methods employ coincidence detection [14,23,36,37], which involves a large number of sequential measurements as well as long data collection times. As a result, these techniques can measure only a limited number of modes in the chosen bases. Thus, in the low-gain SPDC, there is currently no technique that can measure the complete set of Schmidt modes of spatially entangled two-photon fields produced by

*Contact author: radhikap@iitk.ac.in

†Contact author: akjha@iitk.ac.in

 © 2026 American Physical Society

SPDC in situations in which there is no prior knowledge of the Schmidt basis. In this paper, we report a technique that measures the complete set of spatial Schmidt modes and Schmidt spectrum of entangled two-photon states without requiring any prior knowledge of the Schmidt basis or involving coincidence counting.

II. THEORY

The two-photon wavefunction produced by degenerate SPDC, wherein a pump photon (p) with a Gaussian beam profile splits into two photons called the signal (s) and idler (i) inside a nonlinear crystal of thickness L, is given in the transverse momentum basis by [8,10,11,13]

$$\psi_{si}(\boldsymbol{q}_s,\boldsymbol{q}_i) \propto \exp\left[\frac{-|\boldsymbol{q}_s+\boldsymbol{q}_i|^2 w_p^2}{4}\right]\mathrm{sinc}\left[\Delta k_z \frac{L}{2}\right]. \quad (1)$$

Here, $\boldsymbol{q}_s$ and $\boldsymbol{q}_i$ represent the transverse momenta of the signal and idler photons, w_p is the beam waist of the Gaussian pump beam, and Δk_z is the phase-matching parameter [8,10]. The two-photon wavefunction $\psi_{si}(\boldsymbol{\rho}_s,\boldsymbol{\rho}_i)$ in the transverse position basis can be obtained by taking the position-space Fourier transform of Eq. (1), which can be written in the Schmidt decomposed form as [18–20,31,32]

$$\psi_{si}(\boldsymbol{\rho}_s,\boldsymbol{\rho}_i) = \sum_{m,n} \sqrt{\lambda_{mn}}\,\phi_{mn}(\boldsymbol{\rho}_s)\phi^*_{mn}(\boldsymbol{\rho}_i). \quad (2)$$

Here, $\boldsymbol{\rho}_s \equiv (x_s, y_s)$ and $\boldsymbol{\rho}_i \equiv (x_i, y_i)$ denote the transverse position coordinates of the signal and idler photons, respectively, $\phi_{mn}(\boldsymbol{\rho}_s)$ are the Schmidt modes, and $\sqrt{\lambda_{mn}}$ are the Schmidt coefficients, and the set of eigenvalues λ_{mn} is referred to as the Schmidt spectrum. If the Schmidt decomposition contains only one term, the wavefunction $\psi_{si}(\boldsymbol{\rho}_s,\boldsymbol{\rho}_i)$ factorizes, indicating that the two-photon state is separable, that is, not entangled. Therefore, Schmidt-basis analysis provides direct insight into the effective dimensionality and modal structure of an entangled state [39]. We take the partial trace over the idler modes in Eq. (2) and obtain the state of the signal photon in terms of the density matrix element: $W(\boldsymbol{\rho}_s,\boldsymbol{\rho}'_s) = \int \psi_{si}(\boldsymbol{\rho}_s,\boldsymbol{\rho}_i)\psi^*_{si}(\boldsymbol{\rho}'_s,\boldsymbol{\rho}_i)d\boldsymbol{\rho}_i$, which is also referred to as the cross-spectral density function and can be written as

$$W(\boldsymbol{\rho}_s,\boldsymbol{\rho}'_s) = \sum_{m,n} \lambda_{mn}\phi_{mn}(\boldsymbol{\rho}_s)\phi^*_{mn}(\boldsymbol{\rho}'_s). \quad (3)$$

The form of $W(\boldsymbol{\rho}_s,\boldsymbol{\rho}'_s)$ in Eq. (3) is referred to as the coherent mode representation, which represents $W(\boldsymbol{\rho}_s,\boldsymbol{\rho}'_s)$ as an incoherent sum of modes $\phi_{mn}(\boldsymbol{\rho}_s)$ with weights λ_{mn}. Thus, we find that the eigenfunctions and eigenvalues of the cross-spectral density function of the signal photon are the Schmidt modes and Schmidt spectrum of the entangled two-photon state. Therefore, simply by measuring the eigenfunctions and eigenvalues of $W(\boldsymbol{\rho}_s,\boldsymbol{\rho}'_s)$, one can obtain the complete set of Schmidt modes and Schmidt spectrum of the entangled two-photon field. We note that for a pure two-photon state, one can quantify entanglement by measuring the von Neumann entropy of the reduced density matrix corresponding to just one of the photons [40]. Measuring the cross-spectral density function, $W(\boldsymbol{\rho}_s,\boldsymbol{\rho}'_s)$ in our scheme is akin to measuring the reduced density matrix of the two-photon state. Accessing entanglement through one-particle measurement has already been utilized for measuring the Schmidt spectrum in orbital angular momentum [29,41,42], spatial [35,43] and polarization degrees [44] of freedom. Such techniques are highly efficient because Schmidt modes can be obtained by measuring only one of the photons, which results in much higher signal-to-noise ratio and thus high fidelity experimental results.

III. MEASUREMENT SCHEME

Figure 1 is the conceptual illustration of our scheme. The experimental technique, involving a Sagnac-type interferometer, is shown in Fig. 2 [45]. The interferometer

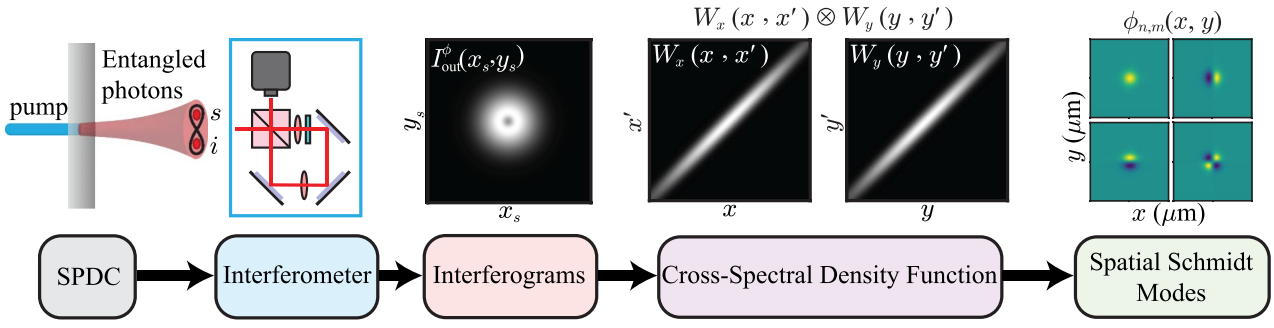


FIG. 1. Conceptual illustration of the scheme. One of the SPDC photons (say, the signal photon) goes through an interferometer which measures its cross-spectral density function $W(\boldsymbol{\rho}_s,\boldsymbol{\rho}'_s)$, which is numerically diagonalized to yield the eigenfunctions $\phi_{mn}(\boldsymbol{\rho}_s)$ and the corresponding eigenvalues λ_{mn}, which are also the Schmidt modes and Schmidt spectrum of the entangled two-photon state $\psi_{si}(\boldsymbol{\rho}_s,\boldsymbol{\rho}_i)$.

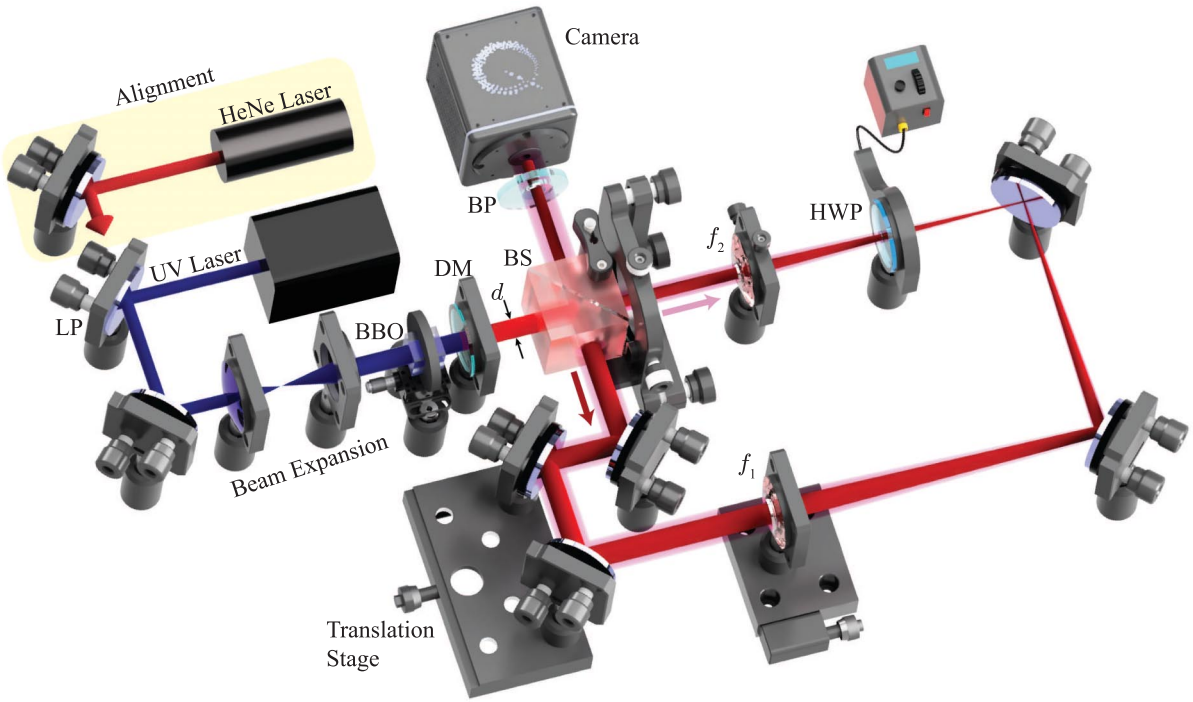


FIG. 2. Experimental setup. LP: Long-pass filter to transmit HeNe and reflect UV; BBO: β-Barium Borate crystal; DM: Dichroic mirror to transmit SPDC photons and block UV; BS: Beam splitter; HWP: Half-wave Plate; BP: Bandpass filter of bandwidth 10 nm centered at 710 nm. HeNe laser is used only for aligning the interferometer and is turned off when UV laser is used. We represent the interfering alternatives with different shades of dark red for the beam reflected at the BS, and light red for the beam transmitted at the BS.

measures any cross-spectral density function $W_s(\boldsymbol{\rho}_s, \boldsymbol{\rho}'_s)$ that is of Schell-model type, that is, any $W_s(\boldsymbol{\rho}_s, \boldsymbol{\rho}'_s)$ that can be expressed as [46]

$$W(\boldsymbol{\rho}_s, \boldsymbol{\rho}'_s) = \sqrt{I(\boldsymbol{\rho}_s) I(\boldsymbol{\rho}'_s)}\, \mu(\boldsymbol{\rho}_s - \boldsymbol{\rho}'_s), \tag{4}$$

where the degree of spatial coherence function $\mu(\boldsymbol{\rho}_s - \boldsymbol{\rho}'_s)$ depends only on the difference coordinate $\boldsymbol{\rho}_s - \boldsymbol{\rho}'_s$. Here, $I(\boldsymbol{\rho}_s) = W(\boldsymbol{\rho}_s, \boldsymbol{\rho}_s)$ is the transverse position probability of the signal photon. The interferometer of Fig. 2 consists of $4f$ lens configuration for magnification and a half-wave plate (HWP) for phase control. The field gets magnified by a factor of $m = f_1/f_2$ in alternative 1 (light red, transmitted twice at the beam splitter) and demagnified by the same factor m in alternative 2 (dark red, reflected twice at the beam splitter). The detection probability $I^{\phi}_{\text{out}}(\boldsymbol{\rho}_s)$ at the camera plane is given by (for details see Ref. [45])

$$I^{\phi}_{\text{out}}(\boldsymbol{\rho}_s) = I(m\boldsymbol{\rho}_s) + I\left(\frac{\boldsymbol{\rho}_s}{m}\right) - 2W\left(m\boldsymbol{\rho}_s, \frac{\boldsymbol{\rho}_s}{m}\right)\cos(4\phi), \tag{5}$$

where $\boldsymbol{\rho}_s$ is the transverse position at the camera plane and ϕ is the HWP angle with respect to the horizontal axis. We take the beam splitter to be 50:50 and the cross-spectral density function $W(m\boldsymbol{\rho}_s, \frac{\boldsymbol{\rho}_s}{m})$ to be real. $I(m\boldsymbol{\rho}_s)$ and $I(\frac{\boldsymbol{\rho}_s}{m})$ are the detection probabilities of the individual interfering alternatives. We note that $W(m\boldsymbol{\rho}_s, \frac{\boldsymbol{\rho}_s}{m})$ can be measured by recording $I^{\phi}_{\text{out}}(\boldsymbol{\rho}_s)$ at $\phi = 0$ and $\phi = \pi/4$, since

$$W\left(m\boldsymbol{\rho}_s, \frac{\boldsymbol{\rho}_s}{m}\right) = \frac{[I^{\phi=\pi/4}_{\text{out}}(\boldsymbol{\rho}_s) - I^{\phi=0}_{\text{out}}(\boldsymbol{\rho}_s)]}{4}. \tag{6}$$

Next, one needs to measure $I(m\boldsymbol{\rho}_s)$ and $I(\frac{\boldsymbol{\rho}_s}{m})$. For this, one needs to remove the beam splitter from the interferometer. This way, field from only one interfering alternative reaches the camera and thus one measures $I(\frac{\boldsymbol{\rho}_s}{m})$. Since it is a common path interferometer, one cannot directly measure $I(m\boldsymbol{\rho}_s)$, but it can be assessed by rescaling the measured $I(\frac{\boldsymbol{\rho}_s}{m})$ by the factor m. The degree of coherence function can therefore be obtained as

$$\mu\left(m\boldsymbol{\rho}_s, \frac{\boldsymbol{\rho}_s}{m}\right) = \frac{W(m\boldsymbol{\rho}_s, \frac{\boldsymbol{\rho}_s}{m})}{\sqrt{I(m\boldsymbol{\rho}_s) I(\frac{\boldsymbol{\rho}_s}{m})}} = \frac{I^{\phi=\frac{\pi}{4}}_{\text{out}}(\boldsymbol{\rho}_s) - I^{\phi=0}_{\text{out}}(\boldsymbol{\rho}_s)}{4\sqrt{I(m\boldsymbol{\rho}_s) I(\frac{\boldsymbol{\rho}_s}{m})}}. \tag{7}$$

We note that although the measured quantities are all intensities and hence involve single-point functions, the degree of coherence function $\mu(m\boldsymbol{\rho}_s, \frac{\boldsymbol{\rho}_s}{m})$ defined above is a two-point correlation function. However, by utilizing the fact that the field is of Schell-model type, we

write: $\mu(m\boldsymbol{\rho}_s, \frac{\boldsymbol{\rho}_s}{m}) = \mu(m\boldsymbol{\rho}_s - \frac{\boldsymbol{\rho}_s}{m}) = \mu[\boldsymbol{\rho}_s(m - \frac{1}{m})]$, which makes it dependent on only one variable. Thus, from the experimentally measured intensities, one can obtain $\mu(m\boldsymbol{\rho}_s - \frac{\boldsymbol{\rho}_s}{m})$ for a given value of m. Next, from the measured values of $\mu[\boldsymbol{\rho}_s(m - \frac{1}{m})]$, one can obtain the two-point degree of coherence function $\mu(\boldsymbol{\rho}, \boldsymbol{\rho}')$, where $\boldsymbol{\rho} = m\boldsymbol{\rho}_s, \boldsymbol{\rho}' = \frac{\boldsymbol{\rho}_s}{m}$, by realizing that the value of $\mu(\boldsymbol{\rho}, \boldsymbol{\rho}')$ for each pair of $(\boldsymbol{\rho}, \boldsymbol{\rho}')$ is related to the single-variable $\boldsymbol{\rho} - \boldsymbol{\rho}'$ as $\mu(\boldsymbol{\rho}, \boldsymbol{\rho}') = \mu(\boldsymbol{\rho} - \boldsymbol{\rho}')$. Once $\mu(\boldsymbol{\rho}, \boldsymbol{\rho}')$ is thus numerically reconstructed, one can numerically obtain the cross-spectral density function $W(\boldsymbol{\rho}, \boldsymbol{\rho}')$ using Eq. (4) and represent it as a matrix over the spatial coordinates. By directly solving the eigenvalue problem associated with this matrix, one obtains the coherent modes of Eq. (3) and thus the Schmidt modes of Eq. (2). This way, by numerically diagonalizing the matrix corresponding to $W(\boldsymbol{\rho}, \boldsymbol{\rho}')$, one obtains the eigenvalues and eigenfunctions of $W(\boldsymbol{\rho}, \boldsymbol{\rho}')$, which correspond to the Schmidt spectrum λ_{mn} and the Schmidt modes $\phi_{mn}(\boldsymbol{\rho})$, respectively.

IV. EXPERIMENT

Figure 2 shows the schematic of the experimental setup. A continuous-wave ultraviolet (UV) laser of wavelength 355 nm and beam waist 507 μm is magnified by a factor of 2 with a 4f lens system (beam expansion in Fig. 2), and the resulting beam of waist $w_p = 1014\,\mu\text{m}$ pumps a type-I β-barium borate (BBO) crystal of length $L = 1$ mm, which produces collinear SPDC photon pairs. A dichroic mirror placed immediately after the crystal blocks the residual UV pump. A $4f$ imaging system with focal lengths $f_1 = 400$ mm and $f_2 = 200$ mm images the crystal plane onto an ORCA-Quest-2 qCMOS camera with a resolution of 4096×2304 pixels and a pixel size of 4.6 μm × 4.6 μm. The imaging system is arranged such that one arm of the interferometer provides a magnification factor of $m = 2$, while the other arm produces a magnification factor of $\frac{1}{m} = \frac{1}{2}$ at the camera plane. In the collinear configuration, the signal and idler fields co-propagate through the interferometer, and thus, the interferogram recorded by the camera is the sum of the interferograms corresponding to both fields. However, since both fields have identical spatial distributions, the recorded interferogram is equivalent to that of either the signal or the idler field. A translation stage is used for adjusting the separation between the lenses f_1 and f_2 to 600 mm. The half-wave plate (HWP) controls the relative phase ϕ, and the interferograms are recorded with an acquisition time of 0.5 s.

V. RESULTS

Figure 3 shows our experimental observations, with the recorded interferograms $I_{\text{out}}^{\phi=\pi/4}(x_s, y_s)$ and $I_{\text{out}}^{\phi=0}(x_s, y_s)$ at $\phi = \pi/4$ and $\phi = 0$ shown in Figs. 3(a) and 3(b), respectively. The difference intensity $I_{\text{out}}^{\phi=\pi/4}(x_s, y_s) - I_{\text{out}}^{\phi=0}(x_s, y_s)$ has been plotted in Fig. 3(c). Figures 3(d) and 3(e) show the recorded intensity plots $I(\frac{x_s}{m}, \frac{y_s}{m})$ and $I(mx_s, my_s)$. Figure 3(f) plots the reconstructed degree of coherence function $\mu(x, x')$, with $m = 2$. We note that $\mu(x, x')$ in Fig. 3(f) depends only on the $x - x'$ coordinate and has no dependence on $x + x'$. This verifies that the

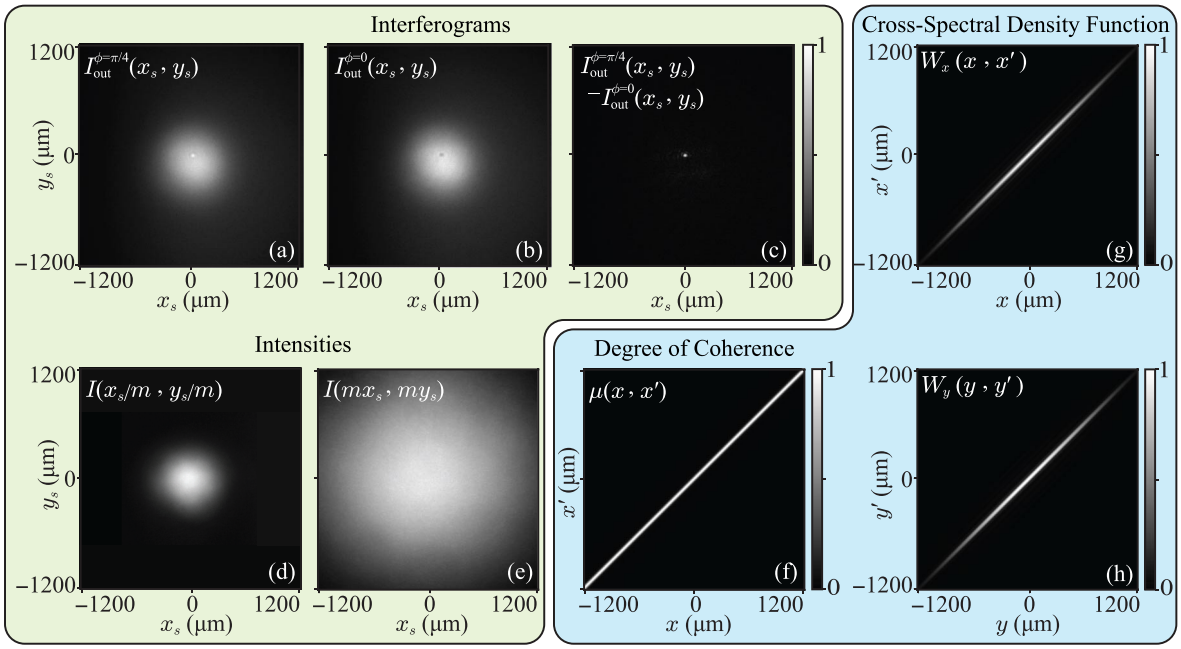


FIG. 3. Experimental observations and reconstructions. (a), (b), (c) are recorded interferograms $I_{\text{out}}^{\phi=\pi/4}(x_s, y_s)$, $I_{\text{out}}^{\phi=0}(x_s, y_s)$, and their difference. (d) and (e) are the intensity profiles corresponding to the magnified and demagnified alternatives. (f) is the reconstructed degree of coherence function $\mu(x, x')$. (g) and (h) are the reconstructed $W_x(x, x')$ and $W_y(y, y')$.

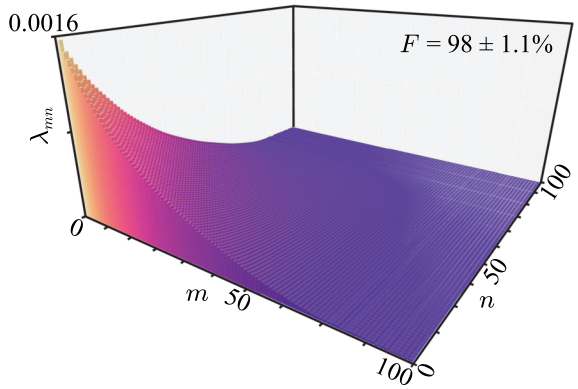


FIG. 4. Reconstructed Schmidt spectrum λ_{mn}. F represents the fidelity of reconstruction. The dimensionality is characterized by the Schmidt number $K = 3413 \pm 39$.

field of the signal photon is of Schell-model type. From the measured functions in Figs. 3(d), 3(e), and 3(f), we reconstruct $W(\boldsymbol{\rho},\boldsymbol{\rho}') \equiv W_x(x,x') \otimes W_y(y,y')$. Figures 3(g) and 3(h) show the reconstructed $W_x(x,x')$ and $W_y(y,y')$, respectively. Next, by diagonalizing $W(\boldsymbol{\rho},\boldsymbol{\rho}')$ in a 100×100 dimensional space, we obtain the Schmidt spectrum λ_{mn} and plot it in Fig. 4. Figure 5 shows the corresponding Schmidt modes $\phi_{mn}(x,y)$ of Eq. (2). Figure 5 presents some representative Schmidt modes up to order 50.

For evaluating the fidelity of our measurement technique, we first numerically construct the theoretical cross-spectral density function from the underlying wavefunction represented by Eqs. (1) and (2). Then by applying the same numerical reconstruction procedure described above on the cross-spectral density function thus obtained, we calculate the theoretical Schmidt modes and spectrum. We then take the experimentally reconstructed Schmidt modes and spectrum reported in Figs. 4 and 5 and calculate the fidelity (F) of the experimentally reconstructed modes in terms of the coefficient of determination defined as [15,47]

$$F \equiv \left[1 - \frac{\sum_n \left(\lambda_n^{(t)} - \lambda_n^{(e)}\right)^2}{\sum_n \left(\lambda_n^{(t)} - \langle \lambda_n^{(t)} \rangle\right)^2}\right] \times 100\%. \tag{8}$$

Here, $\lambda_n^{(t)}$ is theoretical prediction and $\lambda_n^{(e)}$ is experimentally obtained spectrum, and $\langle \ldots \rangle$ denotes mean value.

We find that the measurement fidelity for the Schmidt spectrum in Fig. 4 is about 98% while for the Schmidt modes in Fig. 5 it is up to 99%. The reconstruction fidelity decreases to about 90% for modes of the order of 50, which we ascribe to the finite pixel resolution of the detection camera. We note that we have performed the fidelity measurement experiment several times, the mean value of which has been reported as the fidelity and the associated error is the standard deviation of those

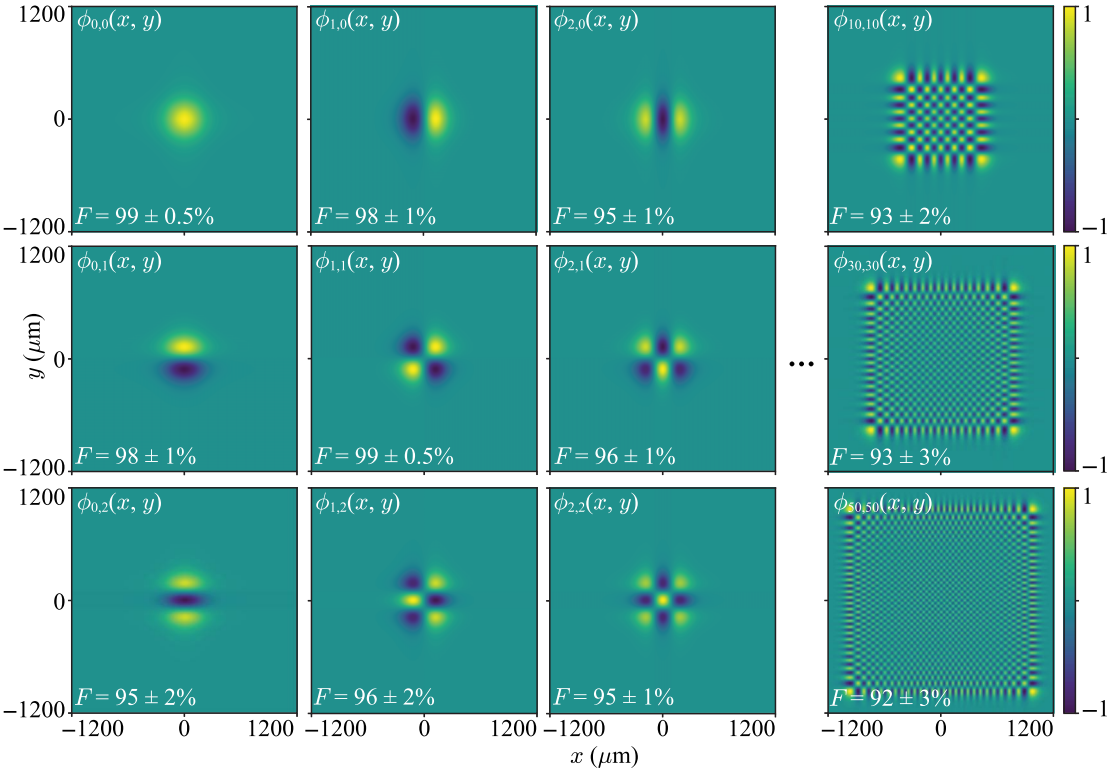


FIG. 5. Plots of experimentally reconstructed Schmidt modes $\phi_{mn}(x,y)$. F is the fidelity of reconstruction.

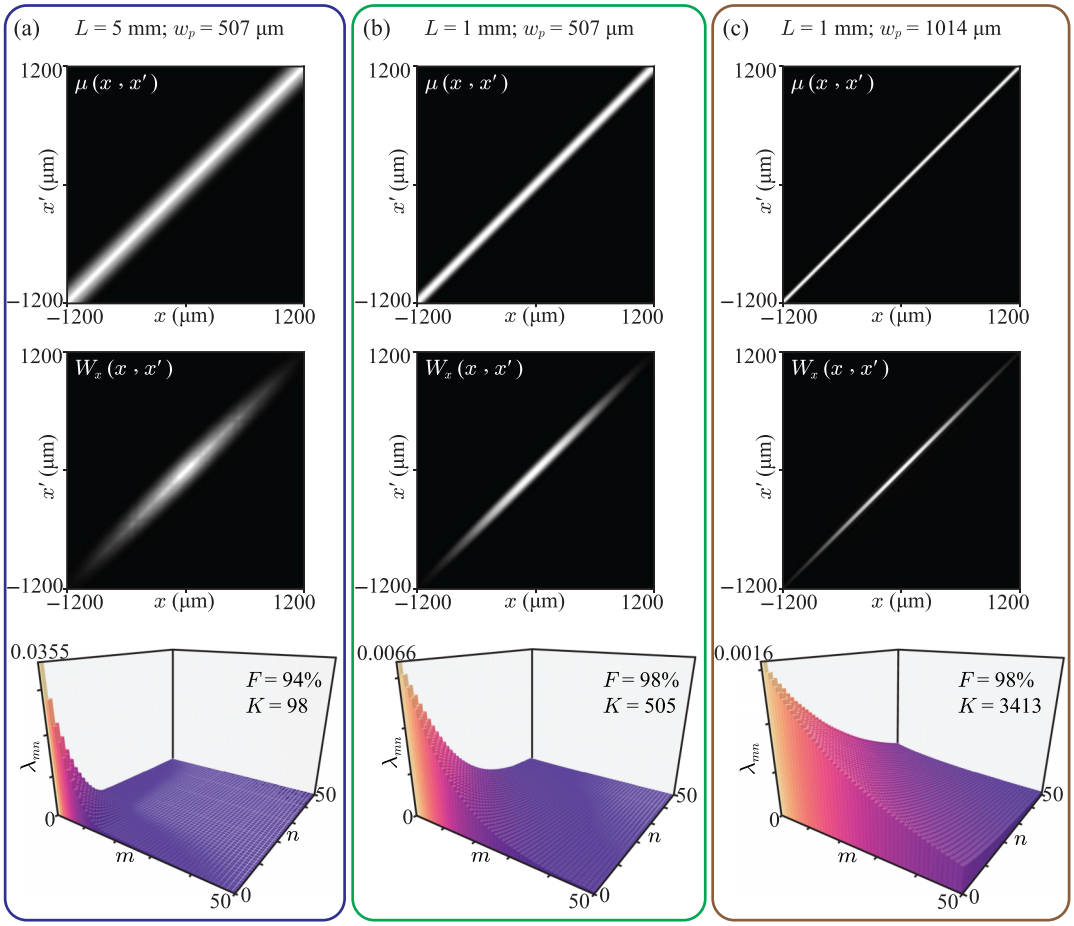


FIG. 6. Experimentally measured Schmidt spectra for various dimensionalities with pump wavelength $\lambda_p = 355$ nm. Top row: Degree of coherence function $\mu(x_s, x_s')$; Middle row: Signal photon cross-spectral density function $W_x(x_s, x_s')$; Bottom row: The corresponding reconstructed Schmidt spectra for (a) $w_p = 507$ μm and $L = 5$ mm; (b) $w_p = 507$ μm and $L = 1$ mm; (c) $w_p = 1014$ μm and $L = 1$ mm.

measurements. From the reconstructed spectrum, we determine the effective mode content of the SPDC state, which yields a Schmidt number $K = 1/\sum_{m,n} \lambda_{mn}^2$ [20] of approximately 3413.

We note that as long as the cross-spectral density function corresponding to the individual photons is of Schell-model type, our scheme works for entangled state of any dimensionality, including the separable state for which there in only one Schmidt mode. In order to demonstrate the applicability of our method for low-dimensional states, we perform experiments with states of various dimensionalities obtained by using various crystal thickness and pump beam waists. Figure 6 shows the experimentally measured $\mu(x, x')$, the cross-spectral density function $W_x(x, x')$, and the corresponding reconstructed Schmidt spectrum. We note for each spectrum the corresponding $\mu(x, x')$ depends only on the difference coordinate $(x - x')$, and thus, the condition for a Schell-model type source is verified. For the three cases shown in the figure, we see that our scheme works with almost perfect fidelity for Schmidt numbers in the range of 98 to 3413. States with low dimensionality are very relevant in the context of generating heralded single photon sources of high spatial purity [48]. Furthermore, our technique works even when the pump field is structured. The corresponding numerical simulations showing the reconstructed Schmidt decomposition are presented in Appendix A.

VI. CONCLUSIONS

In this paper, we have presented a technique for measuring the complete set of spatial Schmidt modes of the high-dimensional entangled two-photon states produced by SPDC without any prior knowledge of the Schmidt basis or requiring coincidence detection. Using this technique, we report measurement of states with over 3000 Schmidt modes and with up to 98% fidelity. To the best of our knowledge, this represents the largest number of spatial Schmidt modes experimentally measured to date. Our technique works even when the entangled field is very low-dimensional or entirely separable as well as when the pump is structured.

Our technique can in principle be extended to nondegenerate SPDC in which one of the entangled photons is in the visible range, while the other one is in the mid-infrared range. In such systems, Schmidt modes can be obtained by making measurements only on the visible photons without requiring demanding mid-infra-red detectors. There have been parallel efforts with partial success at developing spatial mode sorters [10,14,38,49–52]. As a mode sorter allows for the manipulation and control of individual modes in a given basis, our technique, which identifies the Schmidt basis, combined with an appropriate mode sorter, which would sort the Schmidt modes, could enable not only the measurement and characterization of spatial entangled states but also their manipulation and control for the optimal harnessing of high-dimensional advantages.

ACKNOWLEDGMENTS

We acknowledge financial support from the Science and Engineering Research Board through Grants No. STR/2021/000035 and No. CRG/2022/003070, and from the Department of Science & Technology, Government of India through the QuEST Grant No. DST/ICPS/QuST/Theme-I/2019 and the National Quantum Mission (NQM) Grant No. DST/FFT/NQM/QSM/2024/3 for quantum imaging. R. P. and N. S. thank the Prime Minister's Research Fellowship, Ministry of Education, Government of India for financial support.

DATA AVAILABILITY

The data that support the findings of this article are not publicly available. The data are available from the authors upon reasonable request.

APPENDIX: APPLICABILITY OF THE METHOD WITH STRUCTURED PUMPS

The reconstruction technique described in the main text requires the cross-spectral density function of the signal photon to be of Schell-model type, as in Eq. (4);

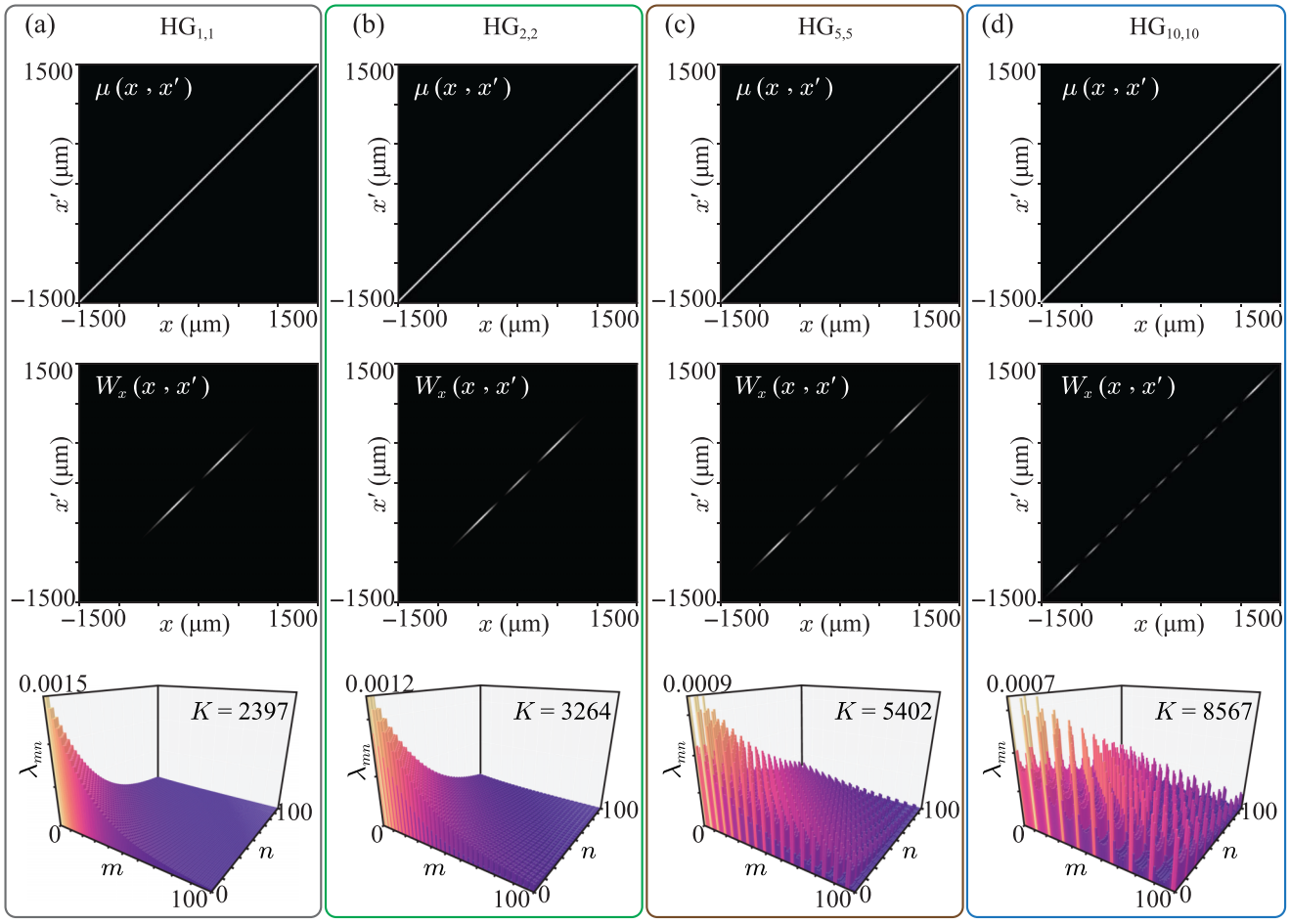


FIG. 7. Numerical simulations of the Schmidt spectra for Hermite-Gauss (HG) structured pumps with pump wavelength $\lambda_p = 355$ nm and pump beam waist $w_p = 507$ μm. Top row: degree of coherence function $\mu(x_s, x_s')$; middle row: signal-photon cross-spectral density function $W_x(x_s, x_s')$; bottom row: the corresponding reconstructed Schmidt spectra. The pump field profiles are (a) $HG_{1,1}$, (b) $HG_{2,2}$, (c) $HG_{5,5}$, and (d) $HG_{10,10}$.

that is, the degree of coherence $\mu(\boldsymbol{\rho}_s - \boldsymbol{\rho}'_s)$ must depend only on the difference coordinate. For type-I, collinear, degenerate SPDC, it can be shown numerically that $W(\boldsymbol{\rho}_s, \boldsymbol{\rho}'_s)$ satisfies this condition [10,46]. In this appendix, we show that the condition continues to hold when the pump has a structured transverse profile, taking higher-order Hermite-Gauss (HG) pump modes as the example, so that the technique applies to such states as well.

Figure 7 shows numerical simulations for $HG_{1,1}$, $HG_{2,2}$, $HG_{5,5}$, and $HG_{10,10}$ pump profiles. The top and middle rows show the degree of coherence and the cross-spectral density function of the signal photon, respectively. In every case, $\mu(x_s, x'_s)$ varies only along the difference coordinate $x_s - x'_s$ and does not change in the orthogonal direction, so the Schell-model condition is satisfied. The Schmidt spectrum can therefore be reconstructed by eigenvalue decomposition of the cross-spectral density function in the same way as in the main text; the resulting spectra are shown in the bottom row of Fig. 7.

[1] J. Wang, J.-Y. Yang, I. M. Fazal, N. Ahmed, Y. Yan, H. Huang, Y. Ren, Y. Yue, S. Dolinar, M. Tur *et al.*, Terabit free-space data transmission employing orbital angular momentum multiplexing, Nat. Photonics **6**, 488 (2012).

[2] N. Bozinovic, Y. Yue, Y. Ren, M. Tur, P. Kristensen, H. Huang, A. E. Willner, and S. Ramachandran, Terabit-scale orbital angular momentum mode division multiplexing in fibers, Science **340**, 1545 (2013).

[3] F. Zhu, M. Tyler, N. H. Valencia, M. Malik, and J. Leach, Is high-dimensional photonic entanglement robust to noise?, AVS Quantum Sci. **3**, 011401 (2021).

[4] S. Ecker, F. Bouchard, L. Bulla, F. Brandt, O. Kohout, F. Steinlechner, R. Fickler, M. Malik, Y. Guryanova, R. Ursin, and M. Huber, Overcoming noise in entanglement distribution, Phys. Rev. X **9**, 041042 (2019).

[5] M. Mirhosseini, O. S. Magaña-Loaiza, M. N. O'Sullivan, B. Rodenburg, M. Malik, M. P. J. Lavery, M. J. Padgett, D. J. Gauthier, and R. W. Boyd, High-dimensional quantum cryptography with twisted light, New J. Phys. **17**, 033033 (2015).

[6] H. Bechmann-Pasquinucci and A. Peres, Quantum cryptography with 3-state systems, Phys. Rev. Lett. **85**, 3313 (2000).

[7] N. J. Cerf, M. Bourennane, A. Karlsson, and N. Gisin, Security of quantum key distribution using d-level systems, Phys. Rev. Lett. **88**, 127902 (2002).

[8] J. Schneeloch and J. C. Howell, Introduction to the transverse spatial correlations in spontaneous parametric down-conversion through the biphoton birth zone, J. Opt. **18**, 053501 (2016).

[9] H. Defienne and S. Gigan, Spatially entangled photon-pair generation using a partial spatially coherent pump beam, Phys. Rev. A **99**, 053831 (2019).

[10] S. Karan, S. Aarav, H. Bharadhwaj, L. Taneja, A. De, G. Kulkarni, N. Meher, and A. K. Jha, Phase matching in β-barium borate crystals for spontaneous parametric down-conversion, J. Opt. **22**, 083501 (2020).

[11] S. P. Walborn, C. H. Monken, S. Pádua, and P. H. Souto Ribeiro, Spatial correlations in parametric down-conversion, Phys. Rep. **495**, 87 (2010).

[12] J. C. Howell, R. S. Bennink, S. J. Bentley, and R. W. Boyd, Realization of the Einstein-Podolsky-Rosen paradox using momentum- and position-entangled photons from spontaneous parametric down conversion, Phys. Rev. Lett. **92**, 210403 (2004).

[13] R. Prasad, S. Wanare, S. Karan, M. K. Joshi, A. Bhattacharjee, and A. K. Jha, Structured position-momentum-entangled two-photon fields, Phys. Rev. Appl. **22**, 064034 (2024).

[14] A. Mair, A. Vaziri, G. Weihs, and A. Zeilinger, Entanglement of the orbital angular momentum states of photons, Nature (London) **412**, 313 (2001).

[15] S. Karan, R. Prasad, and A. K. Jha, Postselection-free controlled generation of a high-dimensional orbital-angular-momentum entangled state, Phys. Rev. Appl. **20**, 054027 (2023).

[16] B. Sephton, A. Vallés, I. Nape, M. A. Cox, F. Steinlechner, T. Konrad, J. P. Torres, F. S. Roux, and A. Forbes, Quantum transport of high-dimensional spatial information with a nonlinear detector, Nat. Commun. **14**, 8243 (2023).

[17] L.-J. Kong, Y. Sun, F. Zhang, J. Zhang, and X. Zhang, High-dimensional entanglement-enabled holography, Phys. Rev. Lett. **130**, 053602 (2023).

[18] F. M. Miatto, T. Brougham, and A. M. Yao, Cartesian and polar Schmidt bases for down-converted photons: How high dimensional entanglement protects the shared information from non-ideal measurements, Eur. Phys. J. D **66**, 183 (2012).

[19] M. A. Nielsen and I. L. Chuang, *Quantum Computation and Quantum Information* (Cambridge University Press, Cambridge, England, 2010).

[20] C. K. Law and J. H. Eberly, Analysis and interpretation of high transverse entanglement in optical parametric down conversion, Phys. Rev. Lett. **92**, 127903 (2004).

[21] M. V. Fedorov and N. I. Miklin, Schmidt modes and entanglement, Contemp. Phys. **55**, 94 (2014).

[22] A. Ekert and P. L. Knight, Entangled quantum systems and the Schmidt decomposition, Am. J. Phys. **63**, 415 (1995).

[23] S. S. Straupe, D. P. Ivanov, A. A. Kalinkin, I. B. Bobrov, and S. P. Kulik, Angular Schmidt modes in spontaneous parametric down-conversion, Phys. Rev. A **83**, 060302(R) (2011).

[24] M. N. O'Sullivan-Hale, I. Ali Khan, R. W. Boyd, and J. C. Howell, Pixel entanglement: Experimental realization of optically entangled d = 3 and d = 6 qudits, Phys. Rev. Lett. **94**, 220501 (2005).

[25] N. Herrera Valencia, V. Srivastav, M. Pivoluska, M. Huber, N. Friis, W. McCutcheon, and M. Malik, High-dimensional pixel entanglement: Efficient generation and certification, Quantum **4**, 376 (2020).

[26] X.-M. Hu, Y. Guo, B.-H. Liu, Y.-F. Huang, C.-F. Li, and G.-C. Guo, Beating the channel capacity limit for superdense coding with entangled ququarts, Sci. Adv. **4**, eaat9304 (2018).

[27] T. Brougham and S. M. Barnett, Information communicated by entangled photon pairs, Phys. Rev. A **85**, 032322 (2012).

[28] Z. Zhang, C. You, O. S. Magaña-Loaiza, R. Fickler, Rde J. León-Montiel, J. P. Torres, T. S. Humble, S. Liu, Y. Xia, and Q. Zhuang, Entanglement-based quantum information technology: A tutorial, Adv. Opt. Photon. **16**, 60 (2024).
[29] G. Kulkarni, R. Sahu, O. S. Magaña-Loaiza, R. W. Boyd, and A. K. Jha, Single-shot measurement of the orbital-angular-momentum spectrum of light, Nat. Commun. **8**, 1054 (2017).
[30] S. Karan, M. P. Van Exter, and A. K. Jha, Broadband uniform-efficiency OAM-mode detector, Sci. Adv. **11**, eadq7201 (2025).
[31] M. V. Fedorov, Y. M. Mikhailova, and P. A. Volkov, Gaussian modelling and Schmidt modes of SPDC biphoton states, J. Phys. B **42**, 175503 (2009).
[32] F. M. Miatto, H. Di Lorenzo Pires, S. M. Barnett, and M. P. van Exter, Spatial Schmidt modes generated in parametric down-conversion, Eur. Phys. J. D **66**, 263 (2012).
[33] V. A. Averchenko, G. Frascella, M. Kalash, A. Cavanna, and M. V. Chekhova, Reconstructing two-dimensional spatial modes for classical and quantum light, Phys. Rev. A **102**, 053725 (2020).
[34] M. Amooei, G. Kulkarni, J. Upham, and R. W. Boyd, Efficient characterization of spatial Schmidt modes of multiphoton entangled states produced from high-gain parametric down-conversion, Phys. Rev. A **111**, 023714 (2025).
[35] V. S. Bhat, K. Bajar, R. Chatterjee, and S. Mujumdar, Facile dual-shot measurement of Schmidt number in type-0 and type-2 downconversion, Phys. Rev. Res. **6**, 033151 (2024).
[36] L. Cohen, E. S. Matekole, Y. Pilnyak, D. Istrati, J. P. Dowling, and H. S. Eisenberg, Measuring the Schmidt number of parametric down conversion by exploiting photon distribution, AVS Quantum Sci. **5**, 025002 (2023).
[37] S. S. Straupe, D. P. Ivanov, A. A. Kalinkin, I. B. Bobrov, S. P. Kulik, and D. Mogilevtsev, Self-calibrating tomography for angular Schmidt modes in spontaneous parametric down-conversion, Phys. Rev. A **87**, 042109 (2013).
[38] H. Qassim, F. M. Miatto, J. P. Torres, M. J. Padgett, E. Karimi, and R. W. Boyd, Limitations to the determination of a Laguerre–Gauss spectrum via projective, phase-flattening measurement, J. Opt. Soc. Am. B **31**, A20 (2014).
[39] C. K. Law, I. A. Walmsley, and J. H. Eberly, Continuous frequency entanglement: Effective finite Hilbert space and entropy control, Phys. Rev. Lett. **84**, 5304 (2000).
[40] V. Vedral, M. B. Plenio, M. A. Rippin, and P. L. Knight, Quantifying entanglement, Phys. Rev. Lett. **78**, 2275 (1997).
[41] A. K. Jha, G. S. Agarwal, and R. W. Boyd, Partial angular coherence and the angular Schmidt spectrum of entangled two-photon fields, Phys. Rev. A **84**, 063847 (2011).
[42] G. Kulkarni, L. Taneja, S. Aarav, and A. K. Jha, Angular Schmidt spectrum of entangled photons: Derivation of an exact formula and experimental characterization for non-collinear phase matching, Phys. Rev. A **97**, 063846 (2018).
[43] H. Di Lorenzo Pires, C. H. Monken, and M. P. van Exter, Direct measurement of transverse-mode entanglement in two-photon states, Phys. Rev. A **80**, 022307 (2009).
[44] S. P. Walborn, P. H. Souto Ribeiro, L. Davidovich, F. Mintert, and A. Buchleitner, Experimental determination of entanglement with a single measurement, Nature (London) **440**, 1022 (2006).
[45] R. Prasad, N. Senapati, S. Karan, A. Bhattacharjee, B. Piccirillo, M. A. Alonso, and A. K. Jha, Experimental technique for measuring radial coherence, Opt. Express **33**, 11693 (2025).
[46] A. Bhattacharjee, S. Biswas, M. A. Alonso, and A. K. Jha, Coherence in the radial degree of freedom, J. Opt. Soc. Am. A **40**, 411 (2023).
[47] S. A. Glantz, B. K. Slinker, and T. B. Neilands, *Primer of Applied Regression & Analysis of Variance*, 3rd ed. (McGraw-Hill Education, New York, 2016).
[48] H.-J. Wu, B.-S. Yu, Z.-H. Zhu, C. Rosales-Guzmán, Z.-Y. Zhou, D.-S. Ding, W. Gao, and B.-S. Shi, Heralded generation of vectorially structured photons with a high purity, Front. Phys. **9**, 654451 (2021).
[49] M. Mirhosseini, M. Malik, Z. Shi, and R. W. Boyd, Efficient separation of the orbital angular momentum eigenstates of light, Nat. Commun. **4**, 2781 (2013).
[50] G. C. G. Berkhout, M. P. J. Lavery, J. Courtial, M. W. Beijersbergen, and M. J. Padgett, Efficient sorting of orbital angular momentum states of light, Phys. Rev. Lett. **105**, 153601 (2010).
[51] R. Sahu, S. Chaudhary, K. Khare, M. Bhattacharya, H. Wanare, and A. K. Jha, Angular lens, Opt. Express **26**, 8709 (2018).
[52] N. R. Heckenberg, R. McDuff, C. P. Smith, and A. G. White, Generation of optical phase singularities by computer-generated holograms, Opt. Lett. **17**, 221 (1992).